arXiv:1708.04414v1 [cond-mat.soft] 15 Aug 2017

Interplay between membrane elasticity and active cytoskeleton forces regulates the aggregation dynamics of the immunological synapse

Nadiv Dharan[1] and Oded Farago[1,2]

[1]*Department of Biomedical Engineering, Ben Gurion University of the Negev, Be'er Sheva 84105, Israel*
[2]*Ilse Katz Institute for Nanoscale Science and Technology, Ben Gurion University of the Negev, Be'er Sheva 84105, Israel*

Adhesion between a T cell and an antigen presenting cell is achieved by TCR-pMHC and LFA1-ICAM1 protein complexes. These segregate to form a special pattern, known as the immunological synapse (IS), consisting of a central quasi-circular domain of TCR-pMHC bonds surrounded by a peripheral domain of LFA1-ICAM1 complexes. Insights gained from imaging studies had led to the conclusion that the formation of the central adhesion domain in the IS is driven by active (ATP-driven) mechanisms. Recent studies, however, suggested that passive (thermodynamic) mechanisms may also play an important role in this process. Here, we present a simple physical model, taking into account the membrane-mediated thermodynamic attraction between the TCR-pMHC bonds and the effective forces that they experience due to ATP-driven actin retrograde flow and transport by dynein motor proteins. Monte Carlo simulations of the model exhibit a good spatio-temporal agreement with the experimentally observed pattern evolution of the TCR-pMHC microclusters. The agreement is lost when one of the aggregation mechanisms is "muted", which helps to identify the respective roles in the process. We conclude that actin retrograde flow drives the centripetal motion of TCR-pMHC bonds, while the membrane-mediated interactions facilitate microcluster formation and growth. In the absence of dynein motors, the system evolves into a ring-shaped pattern, which highlights the role of dynein motors in the formation of the final concentric pattern. The interplay between the passive and active mechanisms regulates the rate of the accumulation process, which in the absence of one them proceeds either too quickly or slowly.

PACS numbers:

I. INTRODUCTION

The adaptive immune system heavily relies upon the ability of T cells to properly interact with antigen presenting cells (APCs). The contact area between the two cells is established by specific receptor-ligand bonds that crosslink the plasma membranes of the T cell and the APC. The key players in this cellular recognition process are T cell receptor (TCR) and lymphocyte function-associated antigen 1 (LFA1) that respectively bind to peptide displaying major histocompatibility complex (pMHC) and intercellular adhesion molecule 1 (ICAM1) embedded in the APC's plasma membrane [1, 2]. During T cell activation, these two types of bonds are redistributed and form a unique geometric pattern of concentric supra-molecular activation centers (SMACs) within approximately 15-30 minutes of the initial contact [3, 4]. In this special arrangement, which is commonly referred to as the immunological synapse (IS), TCR-pMHC bonds are concentrated into a central SMAC (cSMAC), while the LFA1-ICAM1 adhesion bonds form a surrounding ring termed the peripheral SMAC (pSMAC) [5, 6]. This molecular redistribution is thought to play an important role in signal regulation [7], T cell proliferation [8], and focalized secretion of lytic granules and cytokines [9].

Extensive research effort has been devoted to understanding the mechanisms governing the formation of the special architecture of the IS. Mounting evidence from experimental studies point to the actin cytoskeleton as a vital element in controlling the centripetal motion of TCR-pMHC and LFA1-ICAM1 bonds towards their final locations [10]. In the early stages of IS formation, the T cell's actin meshwork reorganizes such that actin-free and actin-rich zone emerge that, later on, constitute the locations of the cSMAC and pSMAC of the IS, respectively. [11]. Moreover, actin polymerization occurring at the periphery of the contact area results in centripetal actin retrograde flow that is crucial for protein translocation [12, 13]. It has been hypothesized that actin retrograde flow produces viscous forces on the intracellular part of TCRs, which lead to their centripetal motion [14–17]. Furthermore, directed transport by dynein motor proteins along the cytoskeleton microtubules has been identified as another ATP-driven process contributing to protein localization in the IS [18, 19]. These experimental evidences have led to the notion that IS formation is governed by active cellular processes related to the cytoskeleton activity.

Interestingly, several theoretical studies have suggested that passive (non-active) mechanisms may also be involved in the formation process of the IS [20–22]. These include (i) receptor-ligand cooperative binding kinetics, and (ii) membrane-mediated attraction. The former is linked to the fact that receptor-ligand binding can only occur when the inter-membrane separation matches the bond length and, thus, new bonds are more likely to form in regions that are already populated by other bonds [23]. The latter is a mechanism of attraction between distant bonds. It is linked to the reduction in fluctuation entropy and increase in curvature elasticity that the mem-

branes experience due to their attachment by the adhesion bonds [24]. The free energy cost is minimized when the adhesion bonds are localized in a single domain which is, therefore, thermodynamically favorable. Specifically to the IS, TCR-pMHC and LFA1-ICAM1 bonds are expected to segregate into two distinct domains due to the marked difference in bond length between them ($\simeq 15\,\mathrm{nm}$ and $\simeq 42\,\mathrm{nm}$, respectively [25]), which causes strong membrane deformation. The interplay between both of these passive mechanisms may result in patterns that are not only extremely similar to those observed experimentally, but also form on biologically relevant timescales [20–22].

From a physical perspective, domain formation induced by membrane-mediated attraction can be viewed as a demixing phase transition [26–28]. In a previous study, we analyzed the membrane-mediated interactions between adhesion bonds and demonstrated that TCR-pMHC can phase separate from LFA1-ICAM1 and form domains with similar densities to those in the IS [29]. However, conventional phase separation theories are insufficient to explain the bullseye pattern of the IS, i.e., the aggregation of TCR-pMHC bonds at the central contact area and the accumulation of LFA1-ICAM1 bonds at the periphery. This very particular structure seems to be directly linked to the activity of the actin cytoskeleton, especially to directed transport of TCR-pMHC by dynein motors along microtubules, and the actin retrograde flow which induces a centripetal force on the TCR-pMHC bonds [30, 31]. It may also be related to the depletion of actin from the center of the contact area, which occurs at the very beginning of the IS formation process. The cytoskeleton is also expected to have a direct influence on the membrane-mediated interactions between the TCR-pMHC bonds. This follows from the attachment of the T cell's membrane to the actin cytoskeleton by various molecules, such as proteins from the ezrin-mesoin-radixin (ERM) family [32], phosphatidylinositol 4,5- bisphosphate (PIP2) [33, 34] and coronin 1 [35]. This coupling between the membrane and the cytoskeleton may modify the shape of the membrane. Here, we extend our previous analysis of the role played by membrane-mediated interactions in formation of TCR-pMHC domains, by including the aforementioned cytoskeleton-related effects, and studying the interplay between the passive and active mechanisms.

A schematic picture of the contact area between the APC and the T cell is depicted in Fig. 1a, showing the two types of adhesion bonds that connect them (the longer LFA1-ICAM1 and shorter TCR-pMHC bonds), the actin cytoskeleton of the T cell including the actin-depleted circular area of radius $\sim 2\,\mu\mathrm{m}$, and the proteins that connect the actin cytoskeleton to the T cell membrane. In order to follow aggregation of the TCR-pMHC central domain, we develop a simple lattice model that constitutes a discrete representation of the system. The lattice model is shown schematically in Fig. 1b. It includes three types of sites: (i) empty (represented by x in Fig. 1b), or

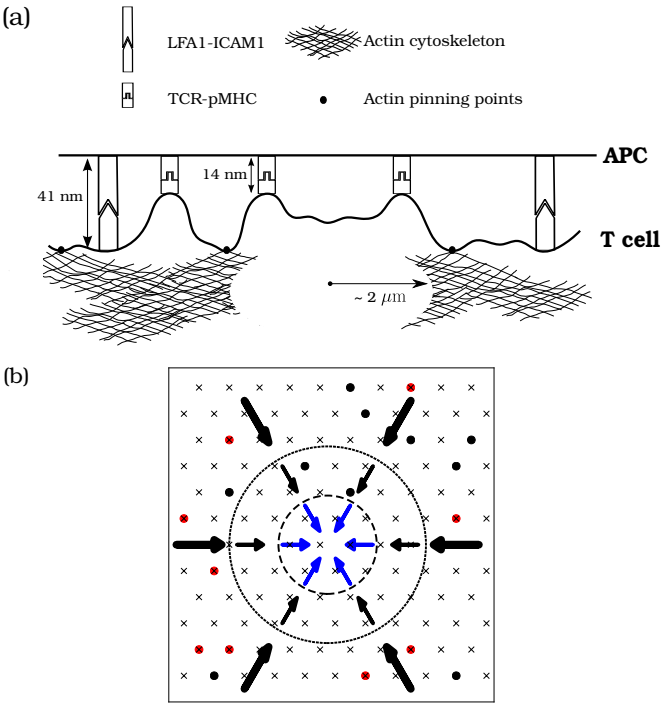


FIG. 1: (a) Schematic of the contact area between the membranes of the T cell and the APC. The two membranes are connected by two types of adhesion proteins: LFA1-ICAM1 and TCR-pMHC with bond lengths of 41 nm and 14 nm, respectively. The T cell's membrane is attached to the cytoskeleton by a set of actin pinning proteins. A central region in the contact area of radius $\sim 2\,\mu\mathrm{m}$ is devoid of actin. (b) The lattice model of the contact area depicted in (a). The lattice sites are either empty (in which case they are marked by the x symbols), or occupied by a single TCR-pMHC bond (black circles) or by a single actin pinning point (red circles). The latter are immobile and are excluded from the actin-depleted central region of the system. The inner dashed circle marks the edge of the central actin-depleted region with radius $R_C = 2\,\mu\mathrm{m}$, while the outer dotted circle marks the edge of the pSMAC, and has a radius $R_P = 4\,\mu\mathrm{m}$. The black and blue arrows represent effective centripetal forces arising from the actin retrograde flow and directed transport by dynein motors, respectively. For $r < R_P$, the magnitude of the active centripetal force is set to $f_0 = 0.1\,\mathrm{pN}$ (small arrows), while for $r > R_P$ the force is set to a twice larger value of $2f_0 = 0.2\,\mathrm{pN}$, and is indicated by large arrows.

singly occupied by either (ii) a mobile point representing a TCR-pMHC bond (black circles in Fig. 1b), or by (iii) an immobile point representing an attachment protein between the membrane and the cytoskeleton (red circles in Fig. 1b). The latter are absent from the actin-depleted central region of the contact area (marked by the dashed circle in Fig. 1b). The membrane-mediated potential of mean force (PMF) between the TCR-pMHC bonds is accounted for via a nearest-neighbor attraction between the mobile points. The cell cytoskeleton is not modeled explicitly in our coarse-grained simulations, but is implicitly introduced via an effective potential that generates the active cytoskeleton forces. These centripetal

forces are represented in Fig. 1b by arrows, and their magnitudes are evaluated in section II C. Since we focus on the aggregation dynamics of TCR-pMHC bonds, we do not study the very rapid remodeling process of the actin cytoskeleton (which is completed within less than a minute from the initial contact between the T cell and the APC [11]), but consider a system where a central actin-depleted region has already been formed.

From the simulation results we conclude that the combination of membrane-mediated attraction, actin retrograde flow, and transport by dynein motors is essential for proper spatio-temporal evolution of the TCR-pMHC bonds. We arrive at this conclusion by performing simulations of systems subjected to only one or two of these driving forces. When only the active cytoskeleton forces are present, the TCR-pMHC bonds individually navigate their way through the immobile pinning points towards the central actin-depleted area. The accumulation process, however, is completed within an extremely short time of several seconds, and does not exhibit formation of peripheral TCR microclusters at early stage. TCR microclusters play a vital role in the T cell response prior to the formation of the cSMAC that triggers TCR down-regulation and signal termination [36–38]. TCR microclusters are observed in simulations taking into account the membrane-induced attraction but neglecting the actin retrograde flow and dynein activity; however, in this case, the aggregation process becomes very slow and proceeds over many hours. In simulations including the membrane-mediated effect and actin retrograde flow but missing the dynein motors, the system evolves into a ring-shaped pattern at the edge of the actin-depleted area. Similar patterns have indeed been observed in a recent experimental study where dynein activity was impaired [19]. Thus, our results corroborate the conclusion that actin retrograde flow drives the centripetal motion of TCR microclusters from the periphery to the center, while dynein motor proteins govern their translocation at the actin-depleted central zone and, therefore, play an essential role in the formation of the final circular bullseye pattern of the IS. When all three mechanisms are present, the central accumulation of the TCR-pMHC bonds occurs within about half an hour, which is indeed the correct biological timescale. The simulations do not only reproduce the experimentally observed values for the timescale of IS formation, but are also able to capture two critical features of this process, namely, (i) the peripheral coarsening of TCR-pMHC into microclusters, and (ii) their subsequent transport towards the center of the contact region. From the simulations we conclude that membrane elasticity and active cytoskeleton forces act as complementary mechanisms that balance each other in a manner that assures an adequate T cell response.

II. MODEL AND SIMULATIONS

A. Lattice-gas model

The accumulation of TCR-MHC bonds at the center of the contact area between a T cell and an APC is studied using a lattice-gas model. In this coarse-grained physical framework, the cell membranes are implicitly accounted for by nearest neighbor interactions that represent the PMF originating from the membrane deformation energy. We consider a triangular lattice with lattice spacing $\xi = 100\,\mathrm{nm}$, which is the range of the membrane-mediated interactions in the system under consideration here (see supplementary information SI1). This sets the spatial resolution of out model, and allows us to ignore direct (e.g., van der Waals and diploar [39]) and lipid-mediated [40] interactions between the various proteins in the system since, typically, the range of these interactinos does not extend beyond $\lesssim 10\,\mathrm{nm}$. The linear size of the system is roughly $L = 10\,\mu\mathrm{m}$ (we simulate a lattice of 99×114 sites with an aspect ratio close to unity), which is representative of the dimensions of the contact area. The model includes two types of lattice points representing the TCR-pMHC bonds (type A) and the membrane-cytoskeleton pinning proteins (type B). The former are mobile, while the latter are located at fixed lattice sites. Both A-A and A-B interactions are purely repulsive at short separations (see SI1), and this feature is accounted for by prohibiting multiple occupancy of a lattice site. At a distance ξ, the A-A interactions are attractive (SI1), and this is represented in the model via a nearest neighbor interaction energy of strength $\epsilon = -4.5\ k_{\mathrm{B}}T$. The value of ϵ is derived from a statistical-mechanical calculation for the membrane-mediated PMF between two TCR-pMHC bonds (SI1). The model does not include explicit representation of the LFA1-ICAM1 bonds. The effect of these bonds is incorporated in the statistical-mechanical calculations of the PMFs through the parameter $h_0 = 27\,\mathrm{nm}$ (SI1), which is the bond length mismatch between LFA1-ICAM1 and TCR-pMHC bonds [41].

The densities of the TCR-pMHC bonds (type A lattice points) and the membrane-cytoskeleton pinning proteins (type B) greatly vary between different experimental works (if reported at all). We therefore set their values in the simulations based on the following considerations: Type A points aggregate to form the cSMAC, which is a circular domain of radius $\sim 2\,\mu\mathrm{m}$ that almost fills (at the end of the process) the actin-depleted central region. The latter includes about 1200 lattice sites, and the number of type A points is set to a slightly smaller value $N_A = 1000$. We note that since the lattice spacing $\xi = 100\,\mathrm{nm}$, the density of the TCR-pMHC bonds in a cluster is $\simeq 80$ bonds/$\mu\mathrm{m}^2$, which is indeed above the threshold density required for full T cell activation [3, 6]. A reasonable estimate to the spacing, l, between membrane-cytoskeleton pinning proteins is a distance of a few hundred nm [42]. In what follows, we show results for systems where the average spacing between

type B points is set to $l = 300\,\mathrm{nm}$. To avoid further complication of our model, we neglect the binding/unbinding kinetics of the membrane-cytoskeleton linkers and assume that the number of type B points is fixed. Nevertheless, we note here that results of simulations with $l = 500\,\mathrm{nm}$ (i.e., with fewer type B points) exhibit negligible differences. The type B points can be found everywhere on the lattice, except for the central actin-depleted region. They are randomly distributed to account for local variations in l, but we do not allow two type B points to occupy nearest-neighbor lattice sites in order to ensure a fairly uniform distribution and avoid type B clusters.

B. Monte Carlo simulations

We perform Monte Carlo (MC) simulations to study the evolution of the lattice model. While MC simulations are designed for statistical ensemble sampling at equilibrium, they can be also used to effectively generate Brownian dynamics in lattice models. The simulations consist of move attempts of a randomly chosen type A point to a nearest lattice site, which is accepted according to the standard Metropolis criterion [43]. During a single MC time unit, τ_{MC}, each type A point experiences (on average) one move attempt. Mapping the MC time unit to real time, t, can be achieved by considering the two-dimensional diffusion relation $\langle r^2\rangle = 4Dt$, where $\langle r^2\rangle$ denotes the mean square displacement and D is the diffusion coefficient. For the MC simulations, each point moves a distances of the lattice spacing $\xi = 100\,\mathrm{nm}$ and, therefore, $\tau_{\mathrm{MC}} = \xi^2/4D$. This can be compared to typical values for the diffusion coefficient of T cell membrane proteins $D \simeq 0.1\ \mu\mathrm{m}^2/\mathrm{sec}$ [44], which yields $\tau_{\mathrm{MC}} \simeq 25$ msec.

C. Active cytoskeleton forces

Similarly to the approach taken in ref. [31], active cytoskeleton processes are not modeled explicitly in our simulations but are instead represented by the effective forces that they induce on the TCR-pMHC bonds. Two active processes are considered, namely (i) actin retrograde flow, and (ii) dynein minus-end directed transport toward the microtubule organizing center (MTOC). These may be viewed as complementary mechanisms since they produce the same net effect of transport toward the center, while operating at different regions of the system. Explicitly, dynein-driven transport governs the dynamics at the central actin-depleted area, while actin-retrograde flow is believed to predominate at the periphery of the system.

Experimental studies reveal that the velocity of the actin retrograde flow towards the center of the contact area achieves a maximal value $v_{\max} \simeq 0.1\ \mu\mathrm{m/sec}$ at the periphery of the contact area. As the flow proceeds toward the center of the contact area, it decreases to approximately $0.5v_{\max}$, and finally vanishes at the edge of the central actin-depleted region [12, 45]. The flow generates a centripetal force on the TCR-pMHC bonds with magnitude proportional to the flow velocity. Inside the actin-depleted region, the centripetal motion of the TCR-pMHC bonds continues, but is now driven by the activity of dynein motors. This has been concluded by experiments showing that in the absence of dynein motor activity, the TCR-pMHC bonds do not penetrate into the actin-depleted region, but instead accumulate around it. Modeling the dynein-induced forces is a highly challenging task since the motor activity depends on many factors, including the concentration of available ATP, the density of dynein motors, and the load opposing the motors which may depend on the size of the transported microcluster. To bypass this issue, we clump all of these factors together into an effective dynein-driven force that acts on individual TCR-pMHC bonds inside the actin-depleted zone, and pulls them towards the center of the system (where the MTOC is located). Experiments suggest that the centripetal velocity of TCR-pMHC bonds transported by both actin retrograde flow and dynein motors is roughly twice larger than the velocity in the absence of motor activity, which suggests that the effective centripetal force induced by both mechanisms is of the same order of magnitude [19]. Taking these various considerations into account, the combined active cytoskeleton forces are introduced to the model via the following effective potential that depends on the distance r from the center of the system

$$\Phi_{\mathrm{active}}(r) = \begin{cases} f_0\, r & r \le R_{\mathrm{P}} \\ 2f_0\,(r - R_{\mathrm{P}}) + f_0 R_{\mathrm{P}} & r > R_{\mathrm{P}}, \end{cases} \qquad (1)$$

where R_P is the outer radius of the pSMAC, which is the region where the flow of actin becomes weaker [45]. This potential generates a centripetal force of magnitude f_0 for $r \le R_{\mathrm{P}}$ and $2f_0$ for $r \ge R_{\mathrm{P}}$. The former region includes the actin-depleted region ($0 < r < R_{\mathrm{C}}$) and the pSMAC ($R_{\mathrm{C}} < r < R_{\mathrm{P}}$), where a force of magnitude f_0 is induced by dynein motor activity and actin retrograde flow, respectively. The latter region corresponds to the periphery of the cell, where actin retrograde flow is stronger and produces an effective force of magnitude $2f_0$. A schematic depicting the forces associated with the potential Φ_{active} at different regions of the contact area is shown in Fig. 1b. Based on confocal images, we set $R_{\mathrm{C}} = 2\,\mu\mathrm{m}$ and $R_{\mathrm{P}} = 4\,\mu\mathrm{m}$ [14]. In order to determine the value of f_0, we use the observation that the actin retrograde flow causes a small peripheral microcluster (a few hundred nanometers in size) to move toward the cell's center at a velocity of $v_c \simeq 20\,\mathrm{nm/sec}$ [46]. We, thus, performed short MC simulations for a single microcluster composed of 10 TCR-pMHC bonds, which is located at the outer region of the system. We measured the velocity of the centripetal movement of the microcluster as a function of f_0, and found that it attains the value of v_c for $f_0 = 0.1\,\mathrm{pN}$. Comparable forces have been

measured in experiments of optically trapped microbeads coupled to actin retrograde flow of similar velocity [47].

III. RESULTS

The spatio-temporal evolution of the system has been analyzed from 10 independent MC runs starting with different random distribution of both type A and B points. Typical snapshots from different stages of the process are shown in Fig. 2, with the type A and B points presented by black and red dots, respectively. At $t = 0$, the type A points are randomly distributed outside of the inner actin-depleted regime (Fig. 2a). Within less than one minute, the type A points coalesce and form small peripheral microclusters consisting of $\lesssim 20$ points (Fig. 2b), which begin to move centripetally. Several type A points have already reached the center system at this stage. The peripheral microclusters are believed to play a vital role in initiating and sustaining TCR signaling [36, 48]. As time proceeds, the clusters further coarsen, which decreases their mobility and slows down their centripetal motion (Figs. 2c-e). The increase in the size of the clusters also causes them to be more affected by the presence of the type B points which act as repelling obstacles. This further restrains the centripetal movement of the microclusters, which have to "navigate" their way through the "curvature corrals" that the type B points form. We also observe in Figs. 2c-e the gradual increase in the size of the central domain, which is the destination where the microclusters accumulate. After 45 minutes (Fig. 2f), almost all type A points reside in the central domain. The dynamics of the MC simulations, as depicted in Figs. 2a-e, closely resembles epifluorescence and total internal reflection fluorescence (TIRF) microscopy images of the IS formation process. Specifically, the microscopy images show the generation of similar microclusters, their drift to the center of the contact area, and their accumulation at the center of the contact area [17, 49]. The simulations exhibit a very good agreement with the experimental observations not only with regard to spatial evolution of the system, but also with respect to the time scales of the different stages of the process. Fig. 2g depicts the percentage of type A points located at in the central domain at the actin-depleted area. About 90% of the lattice points have been accumulated at the center after roughly 40 minutes, which agrees very well with the times reported in the literature for cSMAC formation.

Figs. 2h-j show snapshots from simulations in which dynein activity is turned off. This is done by modifying the effective potential (1) such that $\Phi_{\rm active}\,(r < R_{\rm C}) = f_0\,R_{\rm C} =$ Constant, and thus, the associated force vanishes at the actin-depleted area where the dynein motors operate. For this model system, we observe formation of peripheral microclusters that move centripetally, but do not enter the actin-depleted area. Instead of forming a central quasi-circular domain, the type A points now accumulate in a ring-shaped domain at the edge of the actin-depleted region. Interestingly, very similar ring-like structures have been observed in experiments where dynein activity was inhibited by dynein heavy chain ablation [19]. From the agreement with the experimental results we conclude that cSMAC formation requires that centripetal forces act on the TCR-pMHC bonds in the actin-depleted area, and that the origin of these forces is the action of the dynein motors.

The results displayed in Fig. 2 appears to be in agreement with the widely-held view that the active cytoskeleton forces due to actin retrograde flow and the dynein motors determine the final destination of the TCR-pMHC bonds, which is the center of the cell when dynein activity is enabled and the inner edge of the actin-rich

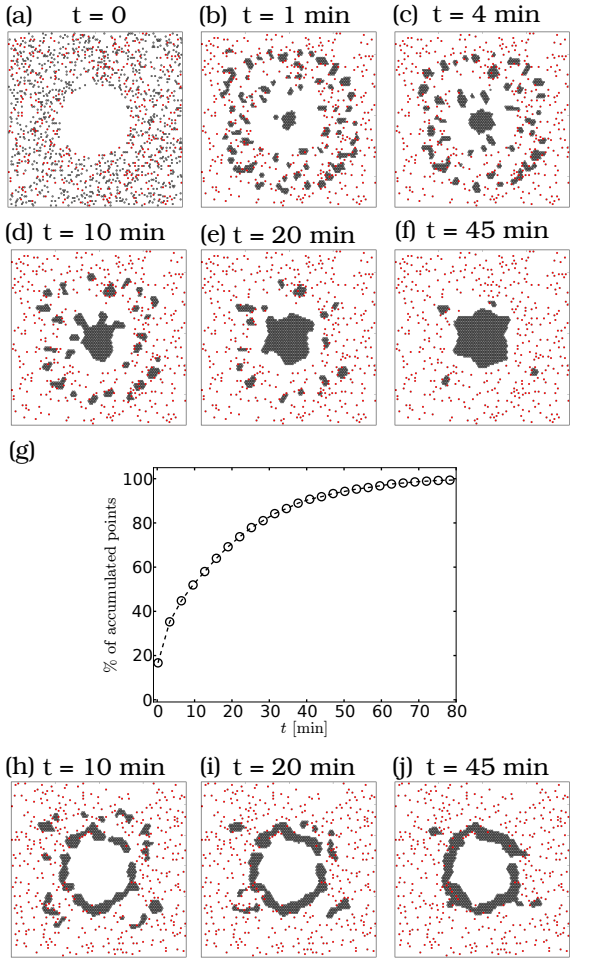


FIG. 2: Simulation snapshots depicting the aggregation process of the TCR-pMHC bonds (type A, black dots) at different times: (a) The random initial distribution, (b-d) early stage formation, coarsening, and centripetal drift of microclusters, and (e,f) late stage accumulation of microclusters and cSMAC formation. The red dots represent the cytoskeleton pinning proteins (type B). (g) The percentage of type A bonds located at the central actin-depleted area as a function of time. (h-j) The evolution of the system in the absence of dynein forces at the center.

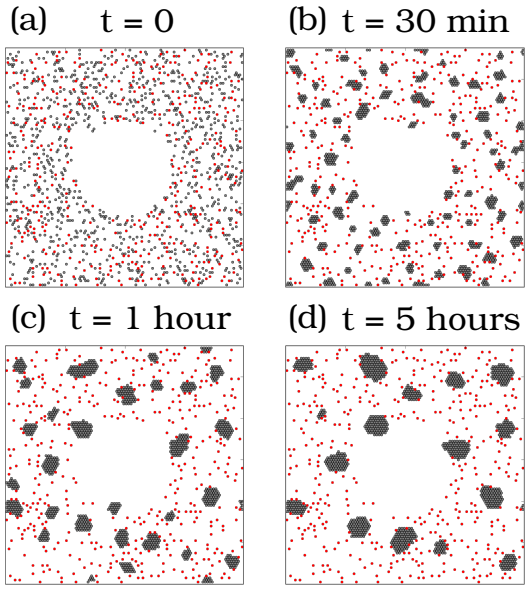


FIG. 3: Simulation snapshots depicting the aggregation process in the absence of active cytoskeleton forces. The type A points form microclusters that, on time scales of hours, barely grow and do not exhibit a drift toward the central area. Color coding as in Fig. 2

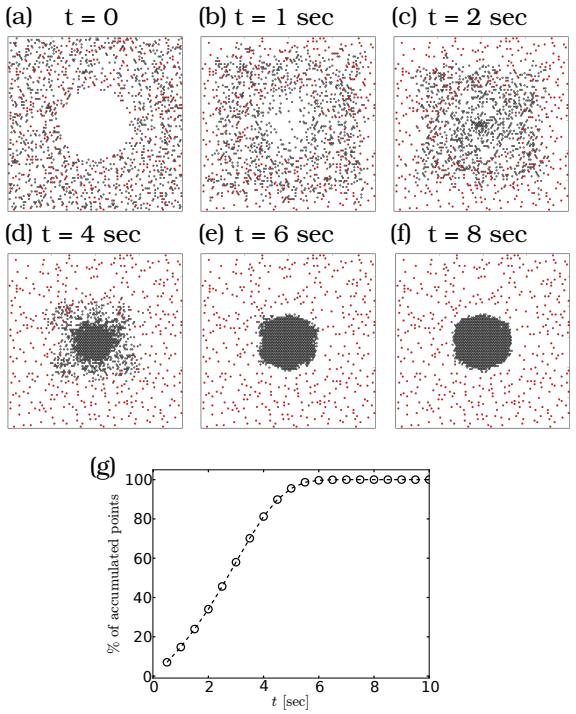


FIG. 4: Simulation snapshots depicting the aggregation process in the absence of membrane-mediated attraction. The type A points do not form microclusters, and accumulate at the central area within a few seconds. Color coding as in Fig. 2. (g) The percentage of type A bonds located at the central actin-depleted area as a function of time.

zone when it is disabled. The results also demonstrate that while a central domain located inside the actin-depleted area constitutes the equilibrium state of the system from a pure thermodynamic perspective, membrane-mediated interactions do not contribute significantly to the centripetal accumulation of the TCR microclusters over the biologically relevant time scales. This is demonstrated in Fig. 3a-d showing snapshots from simulations where $\Phi_{\rm active}$ is completely turned off, leaving the system to evolve only under the influence of the passive membrane-mediated interactions. Neither centripetal motion nor central accumulation of TCR-pMHC bonds are observed in this set of simulations. However, the data seems to indicate that the membrane-mediated interactions play an important role in facilitating the formation and coarsening of peripheral TCR microclusters, which are known to be essential for adequate T-cell immune response. The importance of the passive interactions in inducing the formation of the TCR microclusters is illustrated in Fig. 4, showing snapshots from yet another set of simulations. Here, the nearest-neighbor membrane-mediated attraction between the type A points is muted by setting $\epsilon = 0$, while the effective centripetal potential $\Phi_{\rm active}$ (1) is retained. The simulations reveal that, in this case, the type A points do not form microclusters but instead move individually and quickly accumulate at the center of the system. Since the mobility of a single point is higher than that of a cluster, it is expected that the aggregation process is completed in a shorter time than required in the presence of membrane-mediated attractions. Our computational results show that, indeed, 100% of the points arrive at the central area in less than 6 seconds (see Fig. 4g). We note here that the rate of the accumulation process depicted in Fig. 4 may be exaggerated, since it implies that individual (non-clustered) TCR-pMHC move centrally at a velocity which is about 5 times larger than the velocity of the actin retrograde flow. This problematic dynamic feature is an artifact of the lattice MC dynamics that we employ. Since the focus of interest is the evolution of the system over durations of minutes and hours, the actin retrograde flow force has been calibrated to produce correctly the centripetal velocity of small clusters on these temporal scales - see detailed discussion in section II C. The consequence of this choice is that the velocity of the individual TCR-pMHC bonds turns out to be too high. A reasonable estimation for the centripetal velocity of individual bonds at the periphery of the system is $20 < v < 100$ nm/sec, i.e., higher than the velocity of a single small microcluster but lower than the actin retrograde flow velocity. The accumulation time of bonds moving at such speeds is 0.5-2 minutes, which is still more than an order of magnitude smaller than the IS formation time. Comparing the results of Fig. 4 from simulations that miss the membrane-mediated attraction with Fig. 2 highlights two important aspects of membrane elasticity: First, it facilitates early microcluster formation that play a vital role in T cell activation. Second, they lead to coarsening dynamics that

result in a decrease in the mobility of the clusters and, thereby, regulates the duration of the aggregation process.

IV. DISCUSSION AND SUMMARY

The formation of the immunological synapse (IS) is a complex biological process involving multiple molecular components, including several adhesion proteins, motor proteins, the actin cytoskeleton, and the membranes of both the T cell and the antigen presenting cell. Adhesion between the two cell membranes is established by two types of receptor-ligand bonds, namely, TCR-pMHC and LFA1-ICAM1. At the onset of the process, the T cell's cytoskeleton remodels and an actin-depleted region is formed at the center of the contact area between the cells. Within several tens of minutes, the adhesion bonds segregate such that the TCR-pMHC bonds aggregate into a quasi-circular domain located at the actin-depleted region. The macroscopic time evolution of such a complex system can be only addressed through coarse-grained models employing simplified molecular representation and focusing on the most dominant biophysical mechanisms. Here, we present a minimal computational lattice model aiming to study the dynamics of the TCR-pMHC bonds (represented as lattice points). The model takes into account several forces that emerge in the literature as key factors in TCR-pMHC localization. One is a passive thermodynamic force associated with the membrane curvature energy, which induces attraction between the TCR-pMHC bonds, and provides repulsion between the TCR-pMHC bonds and the proteins connecting the actin cytoskeleton to the membrane. The others are centripetal forces exerted on the TCR-pMHC bonds due to the actin retrograde flow and directed transport by dynein motors along microtubules. These are active (non-equilibrium) forces because the processes that they originate from are driven by consumption of ATP chemical energy.

Our coarse-grained model and MC simulations produce correct evolution dynamics of the IS formation process at the experimentally observed time scales. They thus provide a clear and intuitive picture for the roles played by the main driving forces, and into the intricate interplay between them. Membrane-mediated attraction facilitates the formation of TCR-pMHC microclusters. These microclusters, which initiate biological cues necessary for T cell activation, are rapidly formed and continue to grow by coarsening dynamics over a period of approximately 10 minutes. The TCR-pMHC microclusters are corralled by the membrane-cytoskeleton binding proteins of the T cell, with which they have repulsive membrane-mediated interactions. As the microclusters grow in size, the corralling effect becomes more significant and their diffusivity decreases. This inhibits their accumulation in a central quasi-circular domain, despite the fact that this configuration represents the equilibrium state of the system. What speeds up the dynamics of the microclusters and directs their movement toward the center of the contact area is a centripetal active force induced by actin retrograde flow at the periphery of the synapse. This observation corroborates the largely consensual view about the importance of actin remodeling and retrograde flow for the centripetal translocation of TCR-pMHC bonds at the IS. It is, however, important to emphasize that in simulations without membrane-mediated attraction, a central domain forms very rapidly without exhibiting intermediate microclusters. This observation highlights the, rather overlooked, important role played by the membrane-mediated interactions in regulating the rate of the IS formation process. This novel conclusion drawn from our model and simulations has not been addressed experimentally thus far. A possible setup by which it can be tested is a model system consisting of all the molecular ingredients of the system, except for the LFA1-ICAM1 bonds. This would shut down the membrane-mediated interactions whose origin is is the mismatch in bond length between the TCR-pMHC and the LFA1-ICAM1 bonds.

At the central actin-depleted region, a centripetal force (of magnitude similar to the actin retrograde flow induced force) is effectively generated by dynein motors that walk toward the minus-end of the microtubules. An interesting observation is the formation of a ring-shaped domain at the edge of the actin-depleted region in simulations where this force is turned off. This result is in line with a recent study, in which similar structures were observed when dynein activity was genetically impaired, but actin retrograde flow was maintained. The inability of the system to produce a central circular domain in the absence of dynein activity highlights the role played by the motors at the final stage of the process, where they enable the TCR microclusters to enter the actin-depleted region. Furthermore, the agreement between our simulation results and the experimental data supports the notion presented here of considering two different concentric regions for the active forces, namely a central area dominated by the dynein motors, and a more distant one where the actin retrograde flow is the origin of the centripetal movement of the microclusters.

To conclude, we explored the role played by passive and active forces in the process of IS, and demonstrated how the interplay between them regulates the spatio-temporal pattern formation. Only in simulations where all the driving forces were present, the signature features of the IS formation process were observed. These include microclusters formation and coarsening dynamics, their transport to the central actin-depleted area, and their aggregation into a single quasi-circular domain (the cSMAC). Moreover, the simulated system evolves at the experimentally observed rates: Microclusters are formed within roughly a minute from the beginning of the process, and the final bullseye structure is formed within 15-30 minutes. Our results point to an interesting role of membrane elasticity in regulating the IS formation pro-

cess in a manner that provides T cells with an appropriate time window to allow biological signaling via the peripheral TCR microclusters, which is vital for a proper immune response.

This work was supported by the Israel Science Foundation (ISF) through grant 1087/13.

[1] Alberts B, Jhonson A, Lewis J, Raff M, Roberts K, Walker P (2002) *Molecular Biology of the Cell* (Garland, New York), 4th edition.

[2] Huppa JB, Davis MM (2003) T-cell-antigen recognition and the immunological synapse. *Nat Rev Immunol* 3(12):973-983.

[3] Grakoui A et al. (1999) The immunological synapse: a molecular machine controlling T cell activation. *Science* 285(5425): 221-227.

[4] Johnson KG, Bromley SK, Dustin ML, Thomas ML (2000) A supramolecular basis for CD45 tyrosine phosphatase regulation in sustained T cell activation. *Proc Natl Acad Sci USA* 97(18):10138-10143.

[5] Monks CRF, Freiberg BA, Kupfer H, Sciaky N, Kupfer A (1998) Three-dimensional segregation of supramolecular activation clusters in T cells. *Nature* 395(6697):82-86.

[6] Bromley SK et al. (2001) The immunological synapse. *Annu Rev Immunol* 19(1):375-396.

[7] Mossman KD, Campi G, Groves JT, Dustin ML (2005) Altered TCR signaling from geometrically repatterned immunological synapses. *Science* 310(5751):1191-1193.

[8] Storim J, Bröcker EB, Friedl P (2010) A dynamic immunological synapse mediates homeostatic TCR-dependent and -independent signaling. *Eur J Immunol* 40(10):2741-2750.

[9] Griffiths GM, Tsun A, Stinchcombe JC (2010) The immunological synapse: a focal point for endocytosis and exocytosis. *J Cell Biol* 189(3):399-406.

[10] Dustin ML, Cooper JA (2000) The immunological synapse and the actin cytoskeleton: molecular hardware for T cell signaling. *Nat Immunol* 1(1):23-29

[11] Ritter AT et al. (2015) Actin depletion initiates events leading to granule secretion at the immunological synapse. *Immunity* 42(5):864-876.

[12] Yi J, Wu XS, Crites T, Hammer JA III (2012) Actin retrograde flow and actomyosin II arc contraction drive receptor cluster dynamics at the immunological synapse in Jurkat T cells. *Mol Biol Cell* 23(5):834-852.

[13] Babich A et al. (2012) F-actin polymerization and retrograde flow drive sustained PLCγ1 signaling during T cell activation. *J Cell Biol* 197(6):775-787.

[14] Kaizuka Y, Douglass AD, Varma R, Dustin ML, Vale RD (2007) Mechanisms for segregating T cell receptor and adhesion molecules during immunological synapse formation in Jurkat T cells. *Proc Natl Acad Sci USA* 104(51):20296-20301.

[15] Yu CH, Wu HJ, Kaizuka Y, Vale RD, Groves JT (2010) Altered actin centripetal retrograde flow in physically restricted immunological synapses. *PLoS ONE* 5(7):e11878.

[16] Tskvitaria-Fuller I, Rozelle AL, Yin HL, Wülfing C (2003) Regulation of sustained actin dynamics by the TCR and costimulation as a mechanism of receptor localization. *J Immunol* 171(5):2287-2295.

[17] Hartman NC, Nye JA, Groves JT (2009) Cluster size regulates protein sorting in the immunological synapse. *Proc Natl Acad Sci USA* 106(31):12729-12734.

[18] Schnyder T et al. (2011) B cell receptor-mediated antigen gathering requires ubiquitin ligase Cbl and adaptors Grb2 and Dok-3 to recruit dynein to the signaling microcluster. *Immunity* 34(6):905-918.

[19] Hashimoto-Tane A et al. (2011) Dynein-driven transport of T cell receptor microclusters regulates immune synapse formation and T cell activation. *Immunity* 34(6):919-931.

[20] Qi SY, Groves JT, Chakraborty AK (2001) Synaptic pattern formation during cellular recognition. *Proc Natl Acad Sci USA* 98(12):6548-6553.

[21] Carlson A, Mahadevan L (2015) Elastohydrodynamics and kinetics of protein patterning in the immunological synapse. *PLoS Comput Biol* 11(12):e1004481.

[22] Figge MT, Meyer-Hermann M (2009) Modeling receptor-ligand binding kinetics in immunological synapse formation. *Eur Phys J D* 51(1):153-160.

[23] Krobath H, Różycki B, Lipowsky R, Weikl TR (2009) Binding cooperativity of membrane adhesion receptors. *Soft Matter* 5(17):3354-3361.

[24] Bruinsma R, Goulian M, Pincus P (1994) Self-assembly of membrane junctions. *Biophys J* 67(2):746-750.

[25] Lee SJE, Hori Y, Groves JT, Dustin ML, Chakraborty AK (2002) Correlation of a dynamic model for immunological synapse formation with effector functions: two pathways to synapse formation. *Trends Immunol* 23(10):492-499.

[26] Weikl TR, Asfaw M, Krobath H, Różycki B, Lipowsky R (2009) Adhesion of membranes via receptorligand complexes: Domain formation, binding cooperativity, and active processes. *Soft Matter* 5(17):3213-3224.

[27] Weil N, Farago O (2010) Entropy-driven aggregation of adhesion sites of supported membranes. *Eur Phys J E* 33(1):81-87.

[28] Speck T, Vink RLC (2012) Random pinning limits the size of membrane adhesion domains. *Phys Rev E* 86(3):031923.

[29] Dharan N, Farago O (2016) Formation of semi-dilute adhesion domains driven by weak elasticity-mediated interactions. *Soft Matter* 12(31):6649-6655.

[30] Burroughs NJ, Wülfing C (2002) Differential segregation in a cell-cell contact interface: the dynamics of the immunological synapse. *Biophys J* 83(4):1784-1796.

[31] Weikl TR, Lipowsky R (2004) Pattern formation during T-cell adhesion. *Biophys J* 87(6):3665-3678.

[32] Shaw AS (2001) FERMing up the synapse. *Immunity* 15(5):683-686.

[33] Johnson CM, Rodgers W (2008) Spatial segregation of phosphatidylinositol 4,5-bisphosphate (PIP_2) signaling in immune cell functions. *Immunol Endocr Metab Agents Med Chem* 8(4):349-357.

[34] Sun Y, Dandekar RD, Mao YS, Yin HL, Wülfing C (2011) Phosphatidylinositol (4,5) bisphosphate controls T cell activation by regulating T cell rigidity and organization. *PLoS ONE* 6(11):e27227.

[35] Gatfield J, Albrecht I, Zanolari B, Steinmet MO, Pieters J (2005) Association of the leukocyte plasma membrane with the actin cytoskeleton through coiled coil-mediated

trimeric coronin 1 molecules. *Mol Biol Cell* 16(6):2786-2798.

[36] Varma R, Campi G, Yokosuka T, Saito T, Dustin ML (2006) T cell receptor-proximal signals are sustained in peripheral microclusters and terminated in the central supramolecular activation cluster. *Immunity* 25(1):117-127.

[37] Molnár E, Deswal S, Schamel WWA, (2010) Preclustered TCR complexes. *FEBS Lett* 584(24):4832-4837.

[38] Davis DM, Dustin ML (2004) What is the importance of the immunological synapse? *Trends Immunol* 25(6):323-327.

[39] Israelachvili J, *Intermolecular and Surface Forces* (Academic Press, San Diego), 2nd edition.

[40] Gómez-Llobregat J, Buceta J, Reigada R, (2013) Interplay of cytoskeletal activity and lipid phase stability in dynamic protein recruitment and clustering. *Sci. Rep.* 3:2608.

[41] The utility of this approach was demonstrated in ref. [29], where we employed a more fine-grained lattice model with a microscopic spacing of 5 nm and an explicit representation of the membrane that resulted in TCR-pMHC domains with similar densities to those observed in the IS.

[42] Kusumi A et al. (2012) Dynamic organizing principles of the plasma membrane that regulate signal transduction: commemorating the fortieth anniversary of Singer and Nicolson's fluid-mosaic model. *Annu Rev Cell Dev Biol* 28:215-250.

[43] Metropolis N, Rosenbluth AW, Rosenbluth MN, Teller AH, Teller E (1953) Equation of state calculations by fast computing machines. *J Chem Phys* 21(6):1087-1092.

[44] Favier B, Burroughs NJ, Wedderburn L, Valitutti S (2001) TCR dynamics on the surface of living T cells. *Int Immunol* 13(12):1525-1532.

[45] Kumari S, Curado S, Mayya V, Dustin ML (2014) T cell antigen receptor activation and actin cytoskeleton remodeling. *Biochim Biophys Acta* 1838(2):546-556.

[46] DeMond AL, Mossman KD, Starr T, Dustin ML, Groves JT (2008) T cell receptor microcluster transport through molecular mazes reveals mechanism of translocation. *Biophys J* 94(8):3286-3292.

[47] Mejean CO et al.(2013) Elastic coupling of nascent apCAM adhesions to flowing actin networks. *PLoS One* 8(9):e73389.

[48] Campi G, Varma R, Dustin ML (2005) Actin and agonist MHC-peptide complex-dependent T cell receptor microclusters as scaffolds for signaling. *J Exp Med* 202(8):1031-1036.

[49] Yokosuka T et al. (2005) Newly generated T cell receptor microclusters initiate and sustain T cell activation by recruitment of Zap70 and SLP-76. *Nat Immunol* 6(12):1253-1262.

Supplementary Information 1

Membrane-mediated interactions

The interaction between a T cell and an APC is mediated by several molecular components, especially the cells plasma membranes and the LFA1-ICAM1 and TCR-pMHC adhesion bonds connecting them. In our simulations, we focus on the dynamics of the TCR-pMHC bonds and for this purpose we need to calculate the membrane-mediated interactions that they experience due to the deformation of the membrane of the T cell. To this end, the state of a system that includes all the relevant components, *except for the TCR-pMHC bonds*, is taken as a reference. In this reference state, which is shown schematically in Fig. S1a, the distance between the cells is set by the length of the LFA1-ICAM1 bonds ($\sim$ 41 nm). The deformation energy of the T cell membrane can be described by the Helfrich effective Hamiltonian [1]

$$\mathcal{H} = \int \frac{1}{2}\left[\kappa\left(\nabla^2 h\right)^2 + \gamma h^2\right] d^2\mathbf{r}, \qquad (2)$$

where $h(\mathbf{r})$ is the membrane's height profile relative to the reference plain state at $h = 0$. The first term in eq. (2) is the curvature energy of the membrane, characterized by a bending modulus κ. The second term is a harmonic confining potential of strength γ. This term accounts for various influences that surpress the membrane thermal undulation around $h = 0$, e.g., the interaction of the membrane with the actin cytoskeleton (residing underneath the T cell membrane in Fig. S1a) and the glycocalyx (not shown explicitly). Fig. S1b depicts the same system with the TCR-pMHC included. These pull the T cell membrane toward the APC and locally set the inter-cell separation to 14 nm, thereby deforming the T cell membrane a distance $h_0 = 41 - 14 = 27$ nm from the minimum of the harmonic confining potential. The resulting deformation energy is minimized when the TCR-pMHC bonds aggregate, which is the origin of the attractive membrane-mediated interactions between them. In principle, these interactions are described by a many-body potential of mean force (PMF) that depends on the instataneous coordinates of all TCR-pMHC bonds. In practice, for dilute systems the PMF is well-approximated by the sum of pairwise interactions that depend only on the distance r between the adhesion bonds [2]. The PMF between two TCR-pMHC bonds, $\Phi_{\rm att}(r)$, can be derived from the partition function

$$Z_A = \int \mathcal{D}\left[h(\mathbf{r})\right] e^{-\beta\mathcal{H}} \delta\left(h(0) - h_0\right) \delta\left(h(r) - h_0\right), \qquad (3)$$

which involves statistical averaging over all membrane configurations whose height at the locations of the bonds $(r_1 = 0, r_2 = r)$ is fixed at $h_0 = 27\,\text{nm}$. The height constraints are represented in eq. (3) by the two δ-functions. The partition function can be calculated using standard statistical-mechanics techniques for handling multidimensional Gaussian integrals. The PMF is related to Z_A by $\Phi_{\rm att}(r) = -k_{\rm B}T \ln Z_A$, where $k_{\rm B}$ is the Boltzman constant and T is the temperature. It is given by (see eqs.(5) and (7) in ref. [3])

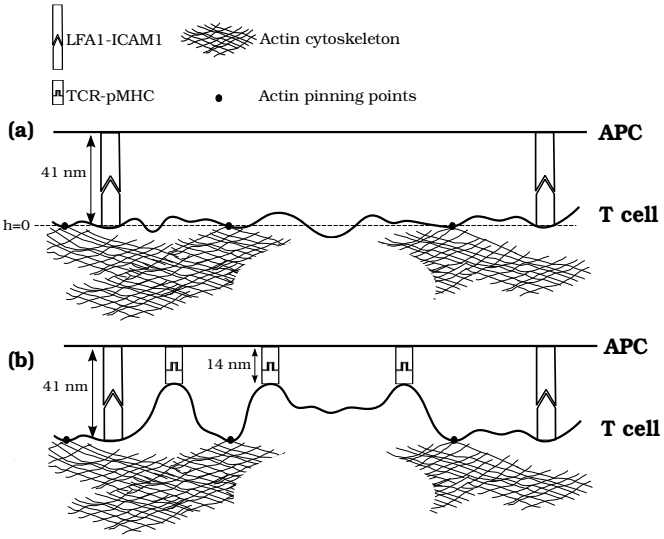


FIG. S1: Schematics of the contact area between the membranes of the T cell and the APC. The two membranes are connected by two types of adhesion proteins: LFA1-ICAM1 and TCR-pMHC with bond lengths of 41 nm and 14 nm, respectively. The T cell's membrane is attached to the cytoskeleton by a set of actin pinning proteins. (a) shows all of the system components except from the TCR-pMHC bonds. The latter, which are present in (b), pull the T cell membrane away from its reference state.

$$\frac{\Phi_{\rm att}(r)}{k_{\rm B}T} = \left(\frac{h_0}{\Delta}\right)^2 \frac{\frac{4}{\pi}\text{kei}\left(\frac{r}{\xi}\right)}{1 - \frac{4}{\pi}\text{kei}\left(\frac{r}{\xi}\right)}, \qquad (4)$$

where kei(x) is the Kelvin function [4], $\xi = (\kappa/\gamma)^{1/4}$ and $\Delta^2 = k_{\rm B}T/8\sqrt{\kappa\gamma}$. Both ξ and Δ have units of length. For T cells, their values are roughly given by $\xi \simeq 100\,\text{nm}$ and $\Delta \simeq 8\,\text{nm}$ [3]. The PMF, $\Phi_{\rm att}/k_{\rm B}T$ (expressed in units of the thermal energy), is depicted by the solid line in Fig. S2 as a function of the normalized pair distance r/ξ, for the aformentioned values of the systems parameters ξ, Δ and h_0. The attractive pair-potential has a strength of a few $k_{\rm B}T$ for $r \simeq \xi$, and is screened at somewhat larger distances.

At separations smaller than ξ, one has to take into account direct excluded volume (hard core) interactions between the TCR-pMHC bonds. Since these are missing in the calculation of the partition function, a purely repulsive potential diverging for $r \to 0$ must be added to $\Phi_{\rm att}$. The full pair potential between TCR-pMHC bonds is reminiscent of a Lennard-Jones potential, i.e., repulsive at very short distances and attractive at an intermediate finite range. Domain formation under the influ-

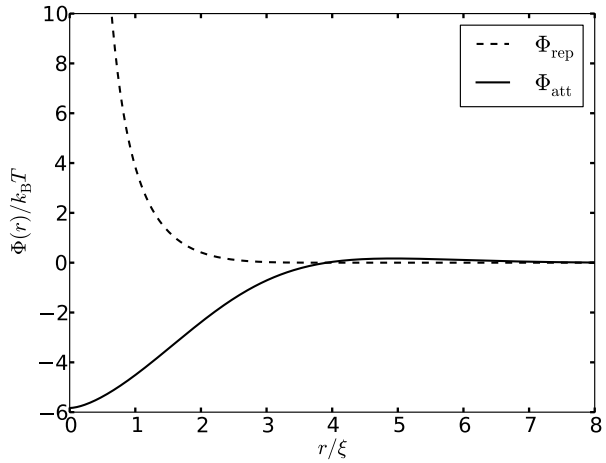


FIG. S2: Curvature-induced interactions: the solid line depicts the curavture-induced attraction between two TCR-pMHC bonds, while the dashed line stands for the curvature-induced repulsion between a TCR-pMHC bond an a membrane-cytoskeleton pinning point.

ence of this type of potentials can be conviniently studied within the framework of the classical discrete lattice-gas (Ising) model where each lattice site can be occupied by at most one lattice point (in order to account for the short range repulsion), and with nearest-neighbor attraction of strength ϵ. Setting the lattice spacing to ξ, we take $\epsilon = \Phi_{\rm att}(r = \xi) \simeq -4.5\ k_{\rm B}T$. We do not consider next-nerarest-neighbor interactions, despite of the fact that the $\Phi_{\rm att}$ does not fully decay at $r = \xi$. The reason for this decision is the many-body nature of the membrane-mediated PMF, which becomes important at the onset of the formation of adhesion clusters. In high density domains, each adhesion bond interacts with the proximal bonds in the first surrounding shell, whose very presence screens the interactions with the slightly more distant bonds in the next shells [5].

Another important note about the many-body membrane-mediated PMF between TCR-pMHC bonds is that, in principal, it should also be dependent on the density of the LFA1-ICAM1 bonds since their presence is the source of effective attraction between the TCR-pMHC bonds. Here, the LFA1-ICAM1 bonds are not modeled explicitly but are represented by the uniform harmonic potential in eq. (2). The utility of this approach was demonstrated in a previous study [3], employing a lattice model with a microscopic spacing of 5 nm and an explicit representation of the membrane. In that work we calculated the phase diagram of the system, which exhibits a two-phase region including semi-dilute domains with densities of about 100 bonds per μm^2. These densities are comparable to the estimated density of TCR-pMHC bonds in the IS, and correspond to a typical distance of $\xi = 100$ nm between them. Thus, the uniform harmonic confining potential correctly captures the influence of the LFA1-ICAM1 bonds in inducing the aggregation of the TCR-pMHC bonds in the system. Based on the success of eq. (2) to capture the thermodynamics of the system within a model of finer resolution, we here present a coarser model with lattice spacing ξ, an set the pairwise interactions between TCR-pMHC bonds at this separation to $\epsilon = -4.5\ k_{\rm B}T$, according to eq. (4) (which has been derived from eq. (2)).

In addition to the membrane-mediated interactions between TCR-pMHC bonds, we also need to calculate the pair PMF between the TCR-pMHC bonds and proteins that pin the T cell membrane to the actin cytoskeleton. These interactions are obviously repulsive due to the large differences in the height of the membrane at the locations of these two proteins ($h = 0$ at the pinning sites compared to $h = h_0 = 27\,$nm at the sites of the TCR-pMHC bonds). The repulsive pair PMF can be derived from the partition function

$$Z_B = \int \mathcal{D}\left[h(\mathbf{r})\right] e^{-\beta\mathcal{H}} \delta\left(h(0) - h_0\right) \delta\left(h(r)\right), \qquad (5)$$

which differs from eq. (3) by one height constraint. The resulting repulsive pair PMF is given by

$$\frac{\Phi_{\rm rep}(r)}{k_{\rm B}T} = \frac{1}{2}\left(\frac{h_0}{\Delta}\right)^2 \frac{\left(\frac{4}{\pi}\right)^2 {\rm kei}^2\left(\frac{r}{\xi}\right)}{1 - \left(\frac{4}{\pi}\right)^2 {\rm kei}^2\left(\frac{r}{\xi}\right)} \qquad (6)$$

and is depicted by the dashed line in Fig. S2 for similar values of system parameters. From Fig. S2 it is clear that $\Phi_{\rm rep}$ is a purely repulsive potential of range $r \simeq \xi$ that quickly decays to zero at larger separations. For $r < \xi$, $\Phi_{\rm rep}$ sharply increases similarly to an excluded volume potential. We thus conclude that the membrane curvature itself serves as a source of repulsion between TCR-pMHAC bonds and pinning proteins, which renders the addition of explicit excluded volume (hard core) interactions unnecessary in this case. In the lattice simulations with lattice constant ξ, this strong membrane-mediated repulsion is accounted for by the standard demand that each lattice site can be occupied by no more than a single lattice point.

[1] Helfrich W (1973) Elastic properties of lipid bilayers: theory and possible experiments. *Z Naturforsch C* 28(11):693-703.

[2] Speck T, Reister E, Seifert U (2010) Specific adhesion of membranes: Mapping to an effective bond lattice gas. *Phys Rev E* 82(2):021923.

[3] Dharan N, Farago O (2016) Formation of semi-dilute adhesion domains driven by weak elasticity-mediated inter-

actions. *Soft Matter* 12(31):6649-6655.

[4] Abramowitz M, Stegun IA (1972) *Handbook of Mathematical Functions: with formulas, graphs, and mathematical tables* (Dover, New York).

[5] Weil N, Farago O (2010) Entropy-driven aggregation of adhesion sites of supported membranes. *Eur Phys J E* 33(1):81-87.